PCCP

ROYAL SOCIETY OF CHEMISTRY

PAPER

View Article Online
View Journal | View Issue

Cite this: *Phys. Chem. Chem. Phys.*, 2025, **27**, 2495

Electron–phonon coupling and thermal transport properties of GaN/AlGaN heterojunction under strain regulation†

Jiao Chen,[a] Zumeng Shan,[a] Baoyi Hu,[a] Zhaoliang Wang,*[a] Dawei Tang[b] and Ke Xu[c]

In the study of GaN/AlGaN heterostructure thermal transport, the interference of strain on carriers cannot be ignored. Although existing research has mainly focused on the intrinsic electronic and phonon behavior of the materials, there is a lack of studies on the transport characteristics of the electron–phonon coupling in heterostructures under strain control. This research comprehensively applies first-principles calculations and the Boltzmann transport equation simulation method to deeply analyze the thermal transport mechanism of the GaN/AlGaN heterojunction considering in-plane strain, with particular attention to the regulatory role of electron–phonon coupling on thermal transport. The study found that electron–phonon coupling increases additional phonon scattering and reorganizes phonon frequencies. Strain significantly regulates the degree of electron–phonon coupling in the GaN/AlGaN heterojunction, which is an effective strategy for controlling the thermoelectric properties of semiconductor materials, where compressive strain enhances coupling while tensile strain weakens it. In addition, in-plane stress causes the redistribution of interface charges, leading to the delocalization migration of electrons from Ga and Al regions to the N atoms, reducing localization. Compressive strain drives the migration of electrons from AlGaN to GaN, forming a more stable two-dimensional electron gas, while tensile strain inhibits this migration. Furthermore, compressive strain promotes the increase of phonon frequencies and the reduction of the bandgap, while tensile strain has the opposite effect. Strain optimizes the delocalization of phonon modes, enhancing the role of low-frequency phonons in interface thermal transport. At the same time, in-plane stress, especially compressive stress, suppresses ballistic phonon transport, affecting the non-equilibrium state of phonons. This study not only enriches the understanding of electron–phonon coupling phenomena in GaN/AlGaN heterojunctions but also provides a theoretical basis and guidance for the strain design and device application of semiconductor materials.

Received 9th October 2024,
Accepted 11th November 2024

DOI: 10.1039/d4cp03880k

rsc.li/pccp

1. Introduction

In the fields of semiconductor physics and nanoelectronics, the electronic and phononic transport characteristics of heterojunctions are crucial for the realization of high-performance electronic devices. Wide-bandgap semiconductor materials, represented by GaN, are the rapidly developing third-generation semiconductor materials that have emerged in recent years. They possess superior properties such as a wide bandgap, high breakdown field strength, high saturation electron velocity, and high thermal conductivity, which have found extensive applications in high-power, high-frequency, and high-temperature electronic devices.[1,2] Due to the high conduction band offset and spontaneous polarization between GaN and AlGaN,[3] a two-dimensional electron gas (2DEG) with high mobility, density, and saturation velocity is formed at the heterointerface.[4] Furthermore, due to the difference in lattice constants, tensile or compressive stress exists at the heterojunction, leading to a strain barrier and thus strain-induced or piezoelectric polarization.[5] Based on this, GaN/AlGaN high electron mobility transistors (HEMTs)[6–8] are widely used in high-power high-frequency applications. However, with the

[a] *Thermal Engineering and Power Department, China University of Petroleum, Qingdao 266580, China. E-mail: wzhaoliang@upc.edu.cn*
[b] *Key Laboratory of Ocean Energy Utilization and Energy Conservation of Ministry of Education, Dalian University of Technology, Dalian 116024, China*
[c] *Suzhou Institute of Nano-Tech and Nano-Bionics (SINANO), Chinese Academy of Sciences, Suzhou 215123, China*

† Electronic supplementary information (ESI) available: The main research content, including detailed theoretical models, computational methods, and additional graphical data. These supplementary materials aid readers in gaining a deeper understanding of the electron–phonon coupling and thermal transport properties of GaN/AlGaN heterojunctions under strain regulation. See DOI: https://doi.org/10.1039/d4cp03880k

rapid increase in the thermal flux density of electronic devices, despite the many advantages of GaN/AlGaN-based devices, they also face the challenge of heat dissipation.[9] Currently, the size of individual electronic components is rapidly approaching the scale of the main mean free path of thermal carriers.[10] Therefore, research on the nanoscale properties of thermal carriers is very necessary.

In the field of crystal physics, the transport of charge and heat primarily relies on free electrons and phonons, which are two fundamental quasi-particles. In metals, electrons dominate the thermal conductivity, while in semiconductors and insulators, the role of phonons is more pronounced. Electron–phonon coupling (EPC)[11] affects the mobility and scattering rate of charge carriers, while simultaneously regulating the pathways and efficiency of heat energy transfer, directly impacting device performance. Advances in numerical simulation techniques have deepened our understanding of the thermal transport properties of electrons and phonons. The thermal transport at heterointerfaces is influenced by differences in phonon transmission efficiency, leading to a non-equilibrium distribution of phonon modes near the interface.[12] Moreover, the coupling effect of interface phonons helps to promote inelastic transport processes, causing the phonon modes in the interface region to exhibit non-equilibrium characteristics.[13] Further research based on the phonon Boltzmann transport equation (BTE) has revealed the characteristics of non-equilibrium phonon transport in nanoscale hot spots, where specific types of electron–phonon interactions and ballistic phonon transmission mechanisms jointly determine the non-equilibrium distribution of phonons.[12] Hu *et al.*[14] used an improved high-order harmonic inelastic scattering model to characterize the scattering behavior of interface phonons and found that inelastic scattering significantly enhances the non-equilibrium degree of phonons at the interface. The energy coupling between different carriers at the heterointerface is a key heat transfer pathway. In order to calculate the phonon nonequilibrium effects and ballistic transport near the interface, Cao *et al.*[15] used a modified lattice dynamics method to accurately determine the phonon transmittance. The impact of electron–phonon coupling (EPC) on thermal transport characteristics has been extensively studied in the scattering channels of phonons. The influence of EPC on thermal transport characteristics plays an important role in the lattice thermal conductivity of certain materials in thermal equilibrium, such as the lattice thermal conductivity of silicon, which can be reduced by 45% when the carrier concentration exceeds 10^{19} cm^{-3}.[11] Cao *et al.*[16] calculated EPC using first-principles methods and found that the coupling effect can significantly reduce the lattice thermal conductivity. In graphene, the anharmonic effect of bending acoustic phonons significantly affects the thermal conductivity, and the interaction between phonon–phonon and EPC leads to a weak temperature dependence of the lattice thermal conductivity.[17] The interaction between phonon–phonon and electron–phonon scattering results in a weak temperature dependence of the lattice thermal conductivity.[18] However, the thermal conductivity exhibits a temperature-independent characteristic, which is attributed to the unusually strong coupling between electrons and phonons.[19] Although existing studies have extensively explored the electronic, phononic, and their electron–phonon interactions in intrinsic materials, there is less research on the transport characteristics of electron–phonon coupling in heterostructures, limiting the understanding of complex interface phenomena.

In the GaN/AlGaN heterojunction, strain is an indispensable factor in material preparation and device application. On one hand, due to the mismatch of lattice parameters and differences in thermal expansion coefficients, in-plane strain[20] occurs between the GaN crystal and the substrate. On the other hand, during the practical application of nanodevices, heterojunctions are often influenced by external loads.[21,22] At the same time, strain engineering,[23] as an effective means of material property regulation, can adjust the behavior of electrons and phonons on a microscopic scale by changing the lattice parameters of the material. In particular, in-plane strain has attracted much attention due to its direct impact on the state of electrons and phonons at the heterojunction interface, such as the variation of the 2DEG mobility in GaN with strain.[21] The strain effect not only significantly affects the electronic properties of semiconductors,[24] but also reconstructs the phonon dispersion relationship, thereby affecting the material's thermal conductivity.[25] By linearly controlling biaxial strain, the energy band structure of the heterojunction can be restructured,[26] thereby triggering a transition from semiconductor to metallic state in the material.[27] Applying uniaxial strain can control the polarization direction, thereby regulating the density of bound charges and free electrons at the interface, achieving significant regulation of heat transport.[5] However, how strain finely affects the electron–phonon coupling mechanism, and how this impact further regulates the carrier transport properties of the heterojunction, remains a question that needs in-depth study. However, existing research is mostly focused on the material properties under strain-free conditions, and systematic studies on the electron–phonon coupling effect under strain conditions are relatively less. This article aims to fill this gap by combining density functional theory (DFT) calculations and simulations based on the Boltzmann transport equation (BTE) to deeply explore the impact of in-plane strain on electron–phonon coupling in GaN/AlGaN heterojunctions, and the regulation of electron–phonon coupling on the electronic and phononic transport of the heterojunction.

The aim of this paper is to investigate the effect of in-plane mechanical strain on the electron and phonon transport properties of GaN/AlGaN heterojunctions and how strain modulates the thermal transport properties by affecting the EPC mechanism and hence the thermal transport properties. In this paper, we explore the combination of DFT calculations with EPW software simulations, where we analyze the electron–phonon coupling constant and scattering rate and integrate these parameters into the BTE equation. On the other hand, the phonon and electron properties of GaN and AlGaN with strain and GaN/AlGaN heterojunction are calculated using DFT to obtain kinetic parameters such as group velocity and relaxation time of carriers for the solution of BTE. The effect of strain on electronic properties is analyzed in terms of energy band

reforming and charge transfer. The thermal transport of GaN/AlGaN interfacial structures with in-plane biaxial compressive/tensile strains is simulated using the MHHIM model with BTE. Mode decomposition is utilized to analyze the response of interface phonon non-equilibrium and quasi-ballistic transport to strain. This work extracts electro–phonon coupling information at the atomic level to study the strain-modulated thermal transport properties of heterogeneous interfaces, providing new ideas and theoretical support for designing and managing the electro-thermal properties of semiconductor devices.

2. Numerical simulation details and calculation methods

The physical structure diagram of the GaN/AlGaN heterojunction-based HEMTis shown in Fig. 1(a). The thermal processes within the device include heat generation near the gate and heat conduction from AlGaN to GaN, with the thermal diffusion resistance at the GaN–AlGaN interface primarily governing the heat transfer within the HEMT. Additionally, at the device level, the heterojunction is subject to in-plane mechanical stress, that is, the influence of mechanical strain and residual strain, and the GaN/AlGaN heterojunction has tensile/compressive strain along the face direction. To study the impact of in-plane mechanical strain in the HEMT on the interface electron and phonon transport, in-plane biaxial strain along the polarization axes a and b is induced in the heterojunction by scaling the lattice coefficients.[28] The strain in the material under stress is defined as $\varepsilon = (l - l_0)/l_0$, where l and l_0 are the lattice constants of the system with and without strain, respectively. Fig. 1(b) and (c) show the initial three-dimensional GaN and AlGaN both having a hexagonal wurtzite structure, with lattice constants of 3.189 Å and 5.15 Å, and both having 4 atoms per unit cell. As shown in Fig. 1(d) and (e), the GaN/AlGaN heterostructure is formed along the c-direction, with 8 atoms per unit cell. Furthermore, to avoid interlayer interactions caused by normal periodic mirroring, a vacuum layer of at least 20 Å was set in the z-direction for all structures. The strength of uniaxial tensile (compressive) strain is set between 5% and 10%, with an increment of 5% for each step. For ease of analysis in the following text, the compressive strain strength is denoted as ε_c, and the tensile strain as ε_t.

The Electron–Phonon Wannier (EPW) software[16,29,30] is a module of the Quantum ESPRESSO (QE) software package, designed for studying electron–phonon coupling phenomena in materials, with the aim of efficiently and accurately calculating the electron–phonon interactions in materials. Based on the Wannier function method, EPW computes the electron–phonon coupling matrix elements, transforming complex Brillouin zone integrals into simpler integrals in the Wannier function space, thereby significantly reducing computational costs. This method addresses the issue of high computational requirements for fine sampling grids needed for convergence in calculations. Based on first-principles density functional theory (DFT) calculations, EPW can provide highly accurate computational results. Therefore, we calculated the electron–phonon coupling constants and scattering rates for the strained GaN/AlGaN heterojunction and incorporated the electron–phonon scattering rates into the BTE to simulate and understand the impact of strain on the material's electronic properties and thermal conductivity. We used the Quantum-ESPRESSO software package for structural optimization, self-consistent calculations, and the calculation of phonon dispersion relations. In the calculations, we used norm-conserving pseudopotentials, with 500 iterations, a cutoff energy of 500 Ry, a k-point mesh of 6 × 6 × 6, and a q-point mesh of 3 × 3 × 3. In the EPW calculations, we adopted a Gaussian broadening of 0.05 eV, with coarse k-point and q-point meshes of 18 × 18 × 18 and 12 × 12 × 12, respectively. By applying Matthiessen's rule, the phonon relaxation time produced by electron–phonon scattering

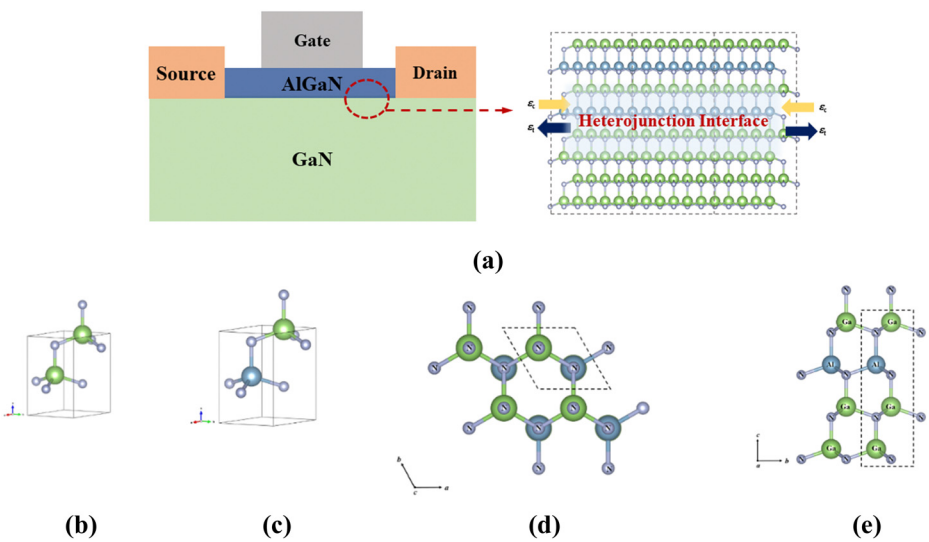

Fig. 1 (a) Schematic atomic structure of the HEMT physical model with heterogeneous interfaces, (b) initial GaN and (c) AlGaN cell, GaN/AlGaN heterojunction: (d) top view perpendicular to the polarization axis c; (e) side view perpendicular to the polarization axis a.

was added to the phonon relaxation time. Through these settings and calculations, we were able to accurately study the electron–phonon coupling phenomena in materials and understand their impact on the material's electronic properties and thermal conductivity.

In this article, DFT calculations include the phonon and electronic properties of strained GaN and AlGaN, as well as the GaN/AlGaN heterojunction. The phonon information part uses the VASP (Vienna Ab initio Simulation Package) software package[31] developed by the Hafner research group at the University of Vienna. The interaction between electrons and ions is described using the projector augmented-wave (PAW)[32] method, and the exchange–correlation functional is described using the Perdew–Burke–Ernzerhof (PBE) form[33] in the generalized gradient approximation (GGA). The computational details for calculating the phonon properties of strained GaN and AlGaN are as follows: during structural relaxation, a Gamma Centered mesh is used to set the density of Brillouin zone sampling points, with a *k*-point mesh of $16 \times 16 \times 16$. Based on density functional perturbation theory (DFPT), a cutoff energy of 520 eV is selected, and the convergence criteria for energy and force are 10^{-8} eV and 10^{-6} eV Å^{-1}, respectively. The finite displacement method[34] is used to perform first-principles calculations on the supercell structures expanded by Phonopy[35] and Thirdorder[36] programs, thereby obtaining the second-order force constant and third-order force constant matrices. The supercell size is $3 \times 3 \times 3$, and the third-order force constant calculations consider the interaction of the nearest 3 atoms. For the GaN/AlGaN heterojunction, the simulation calculations are all centered at the Γ point, with a *k*-point mesh of $12 \times 12 \times 1$, allowing the structure to fully relax until the energy difference convergence criterion reaches 10^{-8} eV and the force reaches 0.01 eV Å^{-1}. The supercell size is $3 \times 3 \times 1$, and the third-order force constant calculations consider the interaction of the nearest 3 atoms. The ShengBTE[36] software package solves the phonon Boltzmann transport equation based on the complete iterative method, without any empirical parameters, and the computational results are well matched with experimental measurements. Therefore, the ShengBTE software is used for anharmonic lattice dynamics calculations, providing the group velocity and relaxation time and other phonon dynamics parameters required for solving the BTE.

This calculation does not consider energy variations along the interface direction; therefore, symmetric boundary conditions are set for the sides perpendicular to the interface, and isothermal boundary conditions are set for the sides parallel to the interface. To minimize computational errors as much as possible, the left boundary temperature is set to 301 K, and the right boundary is set to 300 K, with the distance L from the boundary to the interface at 200 nm. The discrete coordinate method is used to solve the BTE. Combined with the modified Holstein high-order interaction model (MHHIM),[14] the BTE is used to solve the interfacial heat transport process. Although the high-order harmonic interaction model (HHIM)[37] considers the three-phonon interface process on the basis of the diffuse mismatch model (DMM),[38] it only considers the process of two low-frequency phonons combining to produce a high-frequency phonon and does not consider the splitting process of a high-frequency phonon into two low-frequency phonons. The MHHIM model takes into account both of these interface processes, thereby addressing the limitations of HHIM. This method divides the phonons that do not participate in the two-phonon process into two parts: phonons that may participate in the merging process and phonons that may participate in the splitting process. The phonon energy emitted from the interface towards the GaN side is composed of energy reflected back by the three-phonon process, energy transmitted by the two-phonon process, and energy transmitted by the three-phonon process. The proportion of phonons on the GaN side participating in the merging process is shown in eqn (1).[14]

$$\beta_{\mathrm{merge,GaN}}(\omega) = \frac{\alpha_{\mathrm{merge,GaN}}(\omega)}{\alpha_{\mathrm{merge,GaN}}(\omega) + \alpha_{\mathrm{split,GaN}}(\omega)} \tag{1}$$

where $\alpha_{\mathrm{merge,GaN}}$ denotes the transmission coefficient of the merger process in the three-phonon process on the GaN side, $\alpha_{\mathrm{split,GaN}}$ denotes the transmission coefficient of the splitting process. The modified transmission coefficients for the GaN-side merger process are shown in eqn (2)[14] below. The transmission coefficients of the other processes can be calculated in a similar way and the total transmission coefficient can be expressed in eqn (3).[14] Other simulation details are found in Section S1 of the ESI.†

$$\alpha'_{\mathrm{merge,GaN}}(\omega) = \frac{\hbar 2\omega \sum_p (v_2(2\omega,p) D_2(2\omega,p)) f(2\omega)(1-\alpha_2(\omega)) \beta_{\mathrm{merge,AlGaN}}(2\omega)}{\left(\begin{array}{l} 2\hbar\omega \sum_p (v_1(\omega,p) D_1(\omega,p)) f(\omega)(1-\alpha_1(\omega)) \beta_{\mathrm{merge,GaN}}(\omega) + \\ \hbar 2\omega \sum_p (v_2(2\omega,p) D_2(2\omega,p)) f(2\omega)(1-\alpha_2(2\omega)) \beta_{\mathrm{merge,AlGaN}}(2\omega) \end{array} \right)} \tag{2}$$

$$\alpha_1^{\mathrm{MHHIM}} = \beta_{\mathrm{merge,GaN}} \cdot \alpha'_{\mathrm{merge,GaN}} + \beta_{\mathrm{split,GaN}} \cdot \alpha'_{\mathrm{split,GaN}} \tag{3}$$

3. Results and discussion

3.1 The impact of strain on the electron–phonon coupling in GaN/AlGaN heterojunction

Electron–phonon (e–ph) coupling refers to the interaction between electrons and lattice vibrations in a solid, which fundamentally affects the thermoelectric properties of materials. In the GaN/AlGaN heterojunction, electron–phonon coupling not only affects the transfer and scattering rate of charge carriers but also regulates the pathways and efficiency of heat energy transfer. Fig. 2(a) illustrates the thermal conduction mechanisms of e–e scattering, ph–ph scattering, and e–ph coupling in GaN/AlGaN, where ''ph'' denotes phonons and ''e'' denotes free electrons. In the process of solving the BTE, there are various approximation methods, and in this study, we adopt the most basic and widely used Ziman resistivity formula, which relies on the mean of the Eliashberg coupling function to approximate the

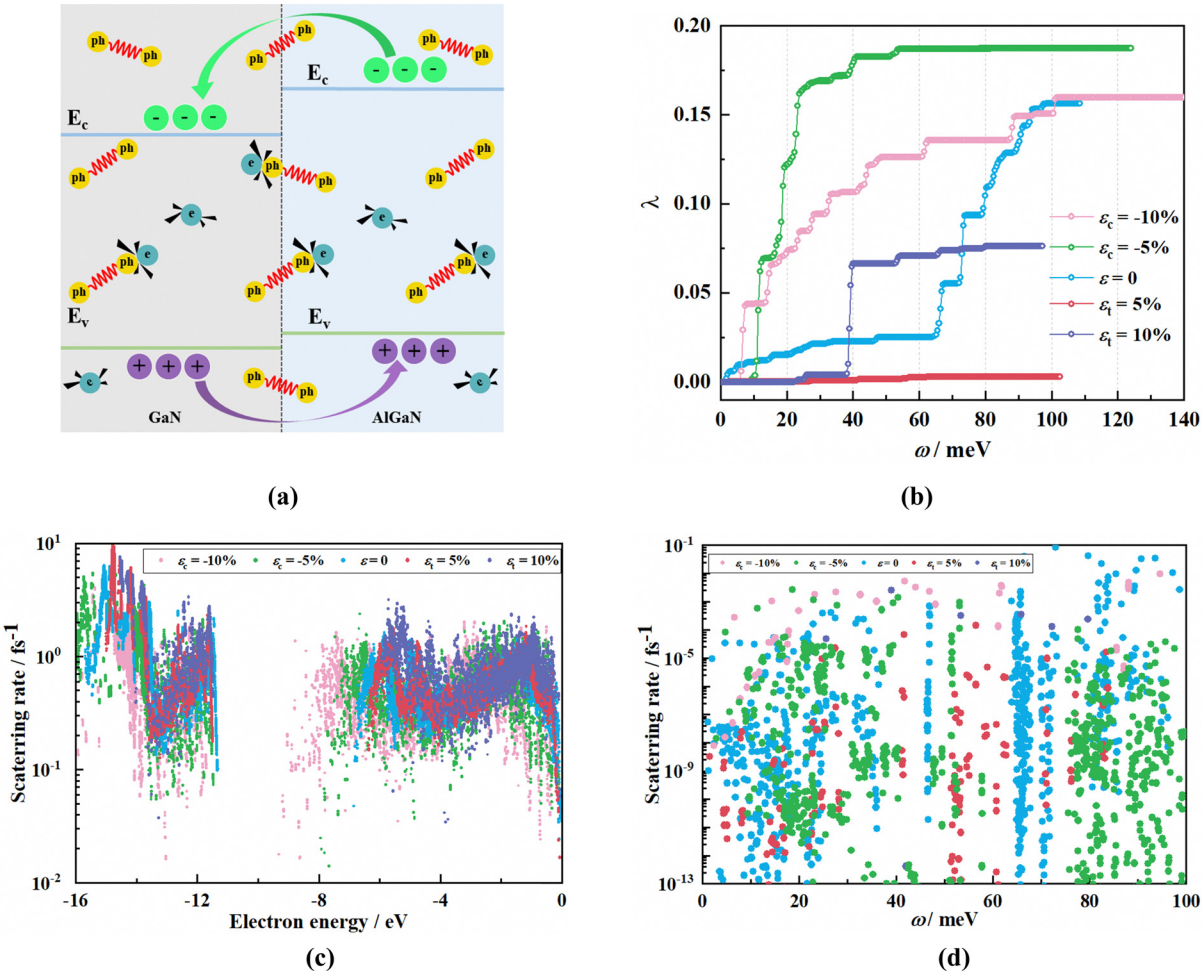

Fig. 2 (a) Schematic diagram of the thermal transport mechanism of GaN/AlGaN, (b) the electron–phonon coupling strength λ of GaN/AlGaN under different strain states, modulated by the strain effect of GaN/AlGaN (c) phonon–phonon scattering rate *versus* (d) the electron–phonon scattering rate with phonon energy.

description of e–ph interaction:

$$\rho = \frac{4\pi m}{ne^2 k_B T} \times \int_0^\infty d\omega \hbar\omega \alpha^2 F(\omega) n(\omega, T)[1 + n(\omega, T)] \quad (4)$$

$$\alpha^2 F(\omega) = \frac{1}{2}\sum \int \frac{d\mathbf{q}}{\Omega} \omega_{\mathbf{q}\nu} \lambda \delta(\omega - \omega_{\mathbf{q}\nu}) \quad (5)$$

where the equations are all expressed in atomic units, $m = \hbar = k_B = 1$, $n(\omega,T)$ is the Bose–Einstein distribution, $F(\omega)$ is Gor'kov's anomalous Green's function, and ω is electron energy. λ[39,40] is the e–ph coupling constant obtained from the momentum and mode integrals of the e–ph coupling strength, ν is the branch index, $\mathbf{q}$ is the wave vector, Ω is the volume of the Brillouin zone, Σ is the electron self-energy, and $\omega_{\mathbf{q}\nu}$ is the frequency.

The e–ph coupling constant (λ) is a measure of the strength of the coupling, and a larger value of λ indicates a stronger interaction between electrons and phonons. In practical applications, semiconductor devices may experience varying degrees of strain due to factors such as manufacturing processes and operating conditions (such as temperature changes, mechanical stress). Additionally, strain engineering is an effective means of regulating the electronic and thermal transport properties of semiconductor materials. Currently, methods such as introducing predetermined strain[40,41] and doping[42] are used to incorporate intrinsic strain into materials or structures. For example, strain is introduced into two-dimensional materials by stretching the substrate by 10% to compressing it by 30%.[41] Therefore, we calculated λ for the GaN/AlGaN heterojunction as the in-plane biaxial strain ε varies from −10% to 10%, with the results shown in Fig. 2(b). In the GaN/AlGaN heterojunction, the e–ph coupling transport process plays a crucial role and is significantly affected by the strain state. Specifically, compressive strain enhances the lattice stiffness and interatomic interactions, leading to an increased degree of e–ph coupling, which not only adds additional phonon scattering opportunities but also causes a reorganization of phonon frequencies. This frequency reorganization may increase the material's thermal conductivity because more phonons participate in the transfer of heat energy. In contrast, tensile strain reduces lattice distortion, lowers the frequency of phonon excitation, and thus significantly decreases the degree of e–ph coupling, reducing scattering events.

Fig. 2(c) and (d) respectively show the e–ph scattering rate and phonon–phonon (ph–ph) scattering rate of the GaN/AlGaN heterojunction under four different strains compared to the free (unstrained) state. Observations reveal the non-uniformity of the e–ph scattering rate, manifesting as multi-valuedness, attributed to the directionality of the scattering process. In solids, the interaction between electrons and phonons depends on their relative wave vectors, leading to different degrees of scattering for electrons with different wave vectors even at the same energy, resulting in diversity of scattering rates. Particularly at the edge of the band gap, the group velocity of the electronic states is reduced to the minimum, making it difficult to achieve effective momentum matching with phonons, leading to a significant reduction in the scattering rate. However, when the electron energy enters the conduction or valence band, the increase in group velocity increases the probability of interaction with phonons, thereby increasing the scattering rate. The e–ph scattering rate of GaN/AlGaN with tensile strain is lower than that in the free (unstrained) and compressive strain states, while compressive strain enhances e–ph interaction. Moreover, the e–ph scattering rate is significantly higher than the ph–ph scattering rate. The coupling strength between electrons and phonons is large, and electrons can effectively polarize the lattice as they move, thereby generating additional phonons. The interaction of electrons with the lattice during the transport process leads to a significant exchange of momentum and energy, especially in charge transport. Additionally, e–ph scattering is a fundamental mechanism in electron transport and has a direct impact on the macroscopic physical properties of materials, while ph–ph scattering, although present, has a relatively smaller impact. Therefore, e–ph scattering plays a more critical role in determining the material's electrical conductivity and other electronic transport properties. Compressive and tensile strains can be used to modulate electron–phonon coupling and optimize thermoelectric properties of semiconductor materials.

3.2 The impact of strain on the electron transport in GaN/AlGaN heterojunction

The band structure of GaN and AlGaN is shown in Fig. S1(a) and (b) (ESI†). The calculated valence band maximum (VBM) and conduction band minimum (CBM) for both GaN and AlGaN are located at the K point, indicating that they are direct bandgap semiconductors. Fig. 2(c) shows the band structure of the GaN/AlGaN heterojunction without strain, from which it can be seen that the VBM and CBM are located at different positions in the Brillouin zone, and the semiconductor properties of GaN and AlGaN are altered after the formation of the heterojunction. The projected electronic band structure of the strained GaN/AlGaN heterojunction is shown in Fig. 3, with the orbital-projected electronic band on the left side of the diagram and the density of states on the right side, with the Fermi level set to 0. It is evident that in-plane biaxial strain not only significantly affects the electronic band structure and the distribution of the density of states in the heterojunction but also changes the high-symmetry point path. As ε varies from −10% to 10%, the bandgap widths are 1.40 eV, 1.72 eV, 2.17 eV, 1.63 eV, and 1.24 eV, respectively. The bandgap width decreases approximately linearly with the increase in the value of ε, meaning that compressive/tensile biaxial strain monotonically increases/decreases the bandgap of the GaN/AlGaN heterojunction. It is worth noting that at ε_c = −10%, both the VBM and

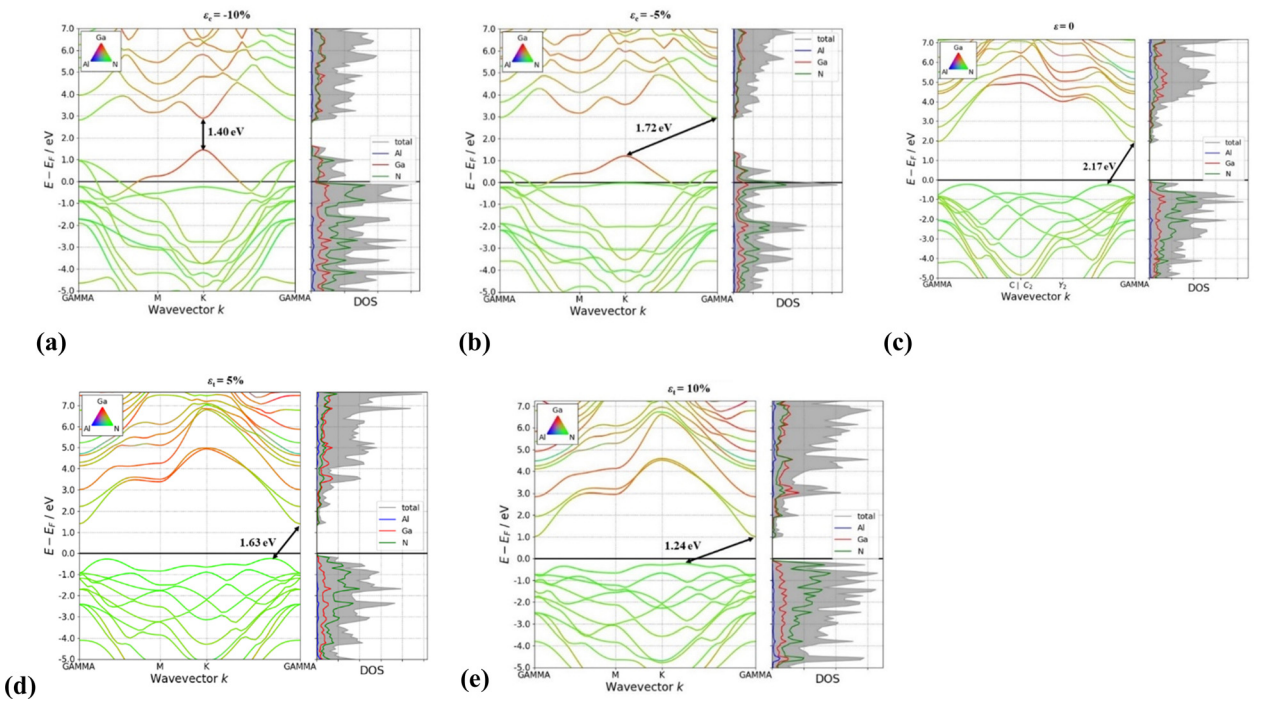

Fig. 3 Projected electronic energy band structure of GaN/AlGaN heterojunction for (a) ε_c = −10%, (b) ε_c = −5%, (c) ε = 0, (d) ε_t = 5% *vs.* (e) ε_t = 10%.

CBM of the GaN/AlGaN heterojunction are located at the K point, indicating a direct bandgap structure. However, for the other structures, the CBM and VBM are located at different positions in the Brillouin zone, and the material becomes an indirect bandgap semiconductor. With the increase of tensile strain, there is band degeneracy in the M–K path of the Brillouin zone, meaning that multiple electronic states have the same energy. Under compressive strain, the lowest conduction band of the heterojunction is restructured, forming multiple peaks. In addition, changes occur in the distribution of the density of states near the Fermi level before and after compression/tension. Under compressive stress, the density of states curve shifts to the right, indicating that the band structure shifts towards a higher energy direction, especially near 1 eV, where the peak of the density of states increases, reflecting an increase in the number of electronic states in this energy range. Under tensile stress, although the overall waveform of the density of states does not change much, the increase in the peak indicates an increase in the number of electronic states near the Fermi level.

The Fermi level is a key concept in semiconductor physics, defining the boundary between filled and unfilled energy states at absolute zero temperature.[43] Above the Fermi level, even if energy levels are filled with electrons, these electrons contribute relatively little to the conductivity of the material. In contrast, the unfilled energy levels below the Fermi level are crucial for conductivity, as electrons can be excited to these levels to participate in the conduction process. When the GaN/AlGaN heterojunction is subjected to in-plane biaxial compressive strain, it causes changes in the lattice constants, which in turn affect the electronic band structure. As the compressive strain increases, the VBM of the heterojunction moves upward. Some energy levels of the valence band may be elevated above the Fermi level, causing electrons above these levels to be partially excited, forming local filling. This local filling changes the electronic distribution of the material, making the contribution of unfilled energy levels below the Fermi level to conductivity more significant. Therefore, the change in the density of states near the Fermi level caused by strain has an important impact on the electronic properties and device performance of the material. As shown in Fig. 2(a), which illustrates the schematic of interface carrier transfer, in the heterojunction, due to the differences in lattice constants and electron affinities between AlGaN and GaN, electrons and holes tend to separate in the two materials. It is observed that since the CBM of GaN is lower than that of AlGaN, electrons are more inclined to gather in the conduction band of GaN, forming a two-dimensional electron gas (2DEG). The valence band holes of GaN are more inclined to gather in AlGaN. This indicates that GaN/AlGaN has a strong interlayer charge transfer. Charge transfer can cause changes in the electric field distribution at the interface, thereby inducing nonlinear changes in the lattice vibration modes, enhancing the anharmonic scattering along the in-plane direction, and thus affecting the transport properties of electrons and phonons.

To further investigate the electron transport behavior of the GaN/AlGaN heterojunction under in-plane stress, we calculated the two-dimensional electron localization function (ELF) at the initial state and under strain levels, as shown in Fig. 4(a). The three-dimensional and two-dimensional combined cross-sectional view of the ELF of the heterojunction in the initial state, as depicted in Fig. S1(c) (ESI†), can clearly distinguish the degree of localization of atoms. The ELF quantifies the probability of electron localization in space, with the isosurface taken at the (1 0 0) crystal plane, with values ranging from 0 to 0.8, where red indicates highly localized electrons and blue indicates less localized electrons. Observations show that the areas near Ga and Al atoms are blue, with ELF values close to 0, indicating that electrons are highly delocalized in these regions. Electrons are mainly localized near N atoms, and the ELF value at the GaN/AlGaN interface is relatively low, suggesting that the interaction at the interface is primarily through weak van der Waals forces rather than strong covalent bonds.[27] Fig. S1(d) (ESI†) illustrates the change in ELF from Ga to N atoms with strain intensity. Under strain conditions, the degree of electron localization around Ga atoms is reduced, indicating that strain has altered the electron distribution. Within the trough range, both compressive and tensile strains decrease the degree of electron localization as the strain intensity increases.

The work function is the minimum energy required for electrons to escape from the surface of a material, and materials with a higher work function have a stronger ability to bind electrons. The work function is defined as: $\Phi = E_{vac} - E_F$, where E_{vac} is the vacuum energy level and E_F is the Fermi level. As shown in Fig. 4(b), Φ_{AlGaN} = 5.602 eV, while Φ_{GaN} = 5.389 eV is 5.389 eV. Due to the higher work function of AlGaN, electrons migrate from AlGaN to GaN to balance the Fermi level. This electron transfer accumulates in the GaN layer, forming a two-dimensional electron gas. In the GaN/AlGaN heterojunction, the difference in ionic radii between Al and Ga, along with the polar covalent bonding of nitrogen atoms, generates polarization charges at the heterojunction interface. The distribution of these polarization charges forms a fixed charge layer at the interface, with the AlGaN layer accumulating positive charges and the GaN layer accumulating negative charges, resulting in an internal electric field from GaN to AlGaN at the heterojunction interface, which causes the electron bands to be restructured. The charge redistribution mechanism at the heterointerface can be further explained by the planar-averaged electrostatic potential (EP). To explore the details of the interfacial interaction in the GaN/AlGaN heterostructure under strain and to gain a deeper understanding of the changes in electron transport under strain, Fig. 4(c) describes the EP of the heterojunction along the *z*-direction. The work function of the GaN/AlGaN heterojunction ($\Phi_{AlGaN/GaN}$) without stress is at 4.875 eV. As the compressive strain intensity increases, $\Phi_{GaN/AlGaN}$ increases from 4.875 eV to 8.024 eV. The work function increases with the degree of compressive strain, but the $\Phi_{GaN/AlGaN}$ under compressive strain is always higher than the Φ_{AlGaN} and Φ_{GaN} without strain. Compressive strain leads to a decrease in lattice constants, causing changes in the electron band structure, increasing the difficulty for electrons to escape from the material surface, and thus increasing the work

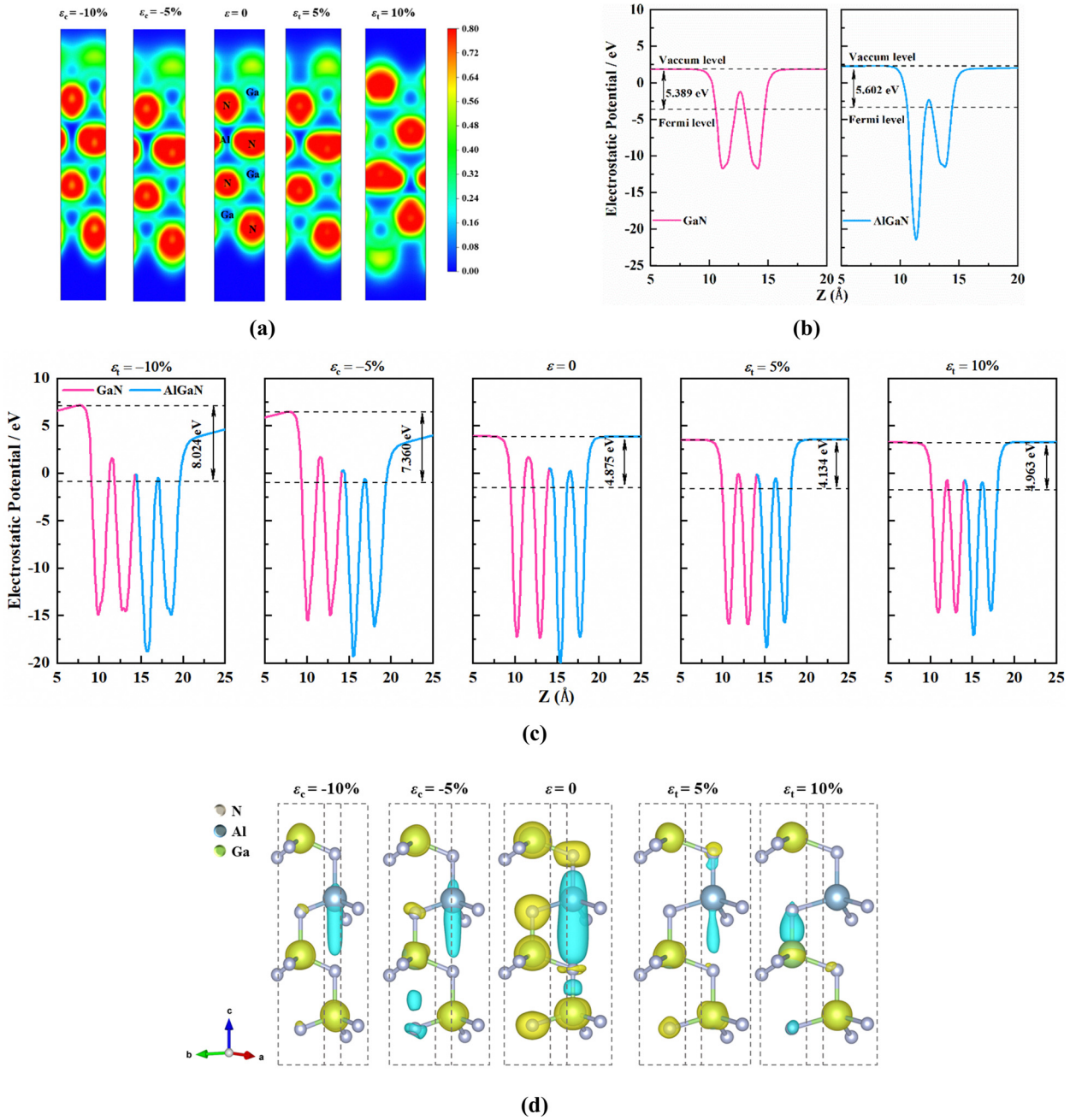

Fig. 4 (a) Cross-section of the ELF of GaN/AlGaN under strain, (b) GaN *vs.* AlGaN figure of merit, (c) plane-averaged electrostatic potentials of GaN/AlGaN for different strain regimes, and (d) three-dimensional charge differential density map of the heterojunction.

function. Moreover, compared with tensile strain, the EP values at both ends are different after applying compressive strain, indicating an asymmetry in the electric potential on both sides of the interface, reflecting the phenomenon of charge redistribution at the interface. On the other hand, as tensile strain increases from 5% to 10%, $\Phi_{GaN/AlGaN}$ increases from 4.134 eV to 4.963 eV, but it is lower than the Φ_{AlGaN} and Φ_{GaN} without strain. Tensile strain causes an increase in lattice constants, making it easier for electrons to escape from the material, thus reducing the work function. However, as tensile strain further increases, the work function slightly rises, possibly due to tensile strain making the lattice structure more stable, leading to a more stable electron distribution. Additionally, due to differences in localized charge distribution, the GaN/AlGaN with strain both exhibit a multi-potential well structure, with both GaN and AlGaN layers containing two potential wells.

As mentioned above, the presence of strain has a significant effect on the electronic properties of heterojunctions. Therefore, we sub-probe the effect of strain on the GaN/AlGaN heterojunction interface properties through the 3D charge differential density. Fig. 4(d) clearly demonstrates the charge redistribution at the interface under strain conditions. The

green region represents charge depletion, while the yellow region represents charge accumulation. The charge transfer at the interface between GaN and AlGaN changes significantly due to van der Waals (vdW) interactions. A large amount of charge depletion is observed at the interface, which indicates the transfer of electrons from AlGaN to GaN and the formation of a two-dimensional electron gas. The charge depletion phenomenon decreases with the increase in the degree of strain. As the strain changes the lattice structure and electronic energy band structure of the material, it affects the charge distribution and migration. Therefore, the formation of high mobility two-dimensional electron gas by strain modulation tunes the energy band structure in order to design high-performance electronic devices.

3.3 The impact of strain on the phonon transport in GaN/AlGaN heterojunction

As shown in the schematic diagram of the GaN/AlGaN heat transport mechanism in Fig. 2(a), the heterojunction not only has electron–electron scattering but also includes ballistic, diffusive, and scattering processes of phonons, as well as electron–phonon coupling transport. Phonons are the quantized representation of lattice vibrations; hence, this section mainly discusses the phonon transport characteristics of GaN/AlGaN with compressive/tenile strain. Fig. 5(a) visualizes the phonon vibrations at the Γ point, where the direction of the arrows indicates the direction of vibration, and the length of the arrows reflects the amplitude of the vibrational mode. It can be observed that strain changes the lattice vibrations of the heterojunction. Fig. S2 (ESI†) and Fig. 6(c) plot the phonon density of states (VDOS) and the phonon dispersion curves along the high-symmetry path Γ → M for the GaN/AlGaN heterojunction, and Fig. 5(b) shows the phonon dispersion curves in the 0–10 THz range. Each GaN/AlGaN unit cell contains 8 atoms, resulting in a total of 24 dispersion curves with different modes in the phonon spectrum, of which 9 are optical branches and 3 are acoustic branches. The acoustic branches can be divided into longitudinal modes (in-plane longitudinal acoustic, LA), in-plane transverse modes (in-plane transverse acoustic, TA), and out-of-plane modes (out-plane transverse acoustic, ZA) according to the direction of lattice vibration. The absence of imaginary frequencies in the dispersion curves indicates that the physical model is dynamically stable within the considered range of strain. The phonon cutoff frequency of GaN/AlGaN increases with the increase in compressive strain strength, with low-frequency phonons blue-shifting and high-frequency phonon modes increasing; whereas it decreases with the increase in tensile strain strength, causing phonons to red-shift. Compressive strain increases the wide bandgap characteristics of the heterojunction, while tensile strain reduces the bandgap.

To further explore the potential mechanisms of strain-controlled interfacial phonon transport, the phonon participation ratio (PPR)[44] is mapped onto the GaN/AlGaN acoustic phonon branches, with the definition of PPR shown in eqn (6):

$$\mathrm{PPR}^{-1} = N\sum_{i}\left(\sum_{\alpha}\varepsilon_{i\alpha}^{*},\lambda\varepsilon_{i\alpha},\lambda\right)^{2} \quad (6)$$

where i sums over all atoms studied, α is the Cartesian direction summed over x, y, z, $\varepsilon_{i\alpha}$ is the vibrational eigenvector

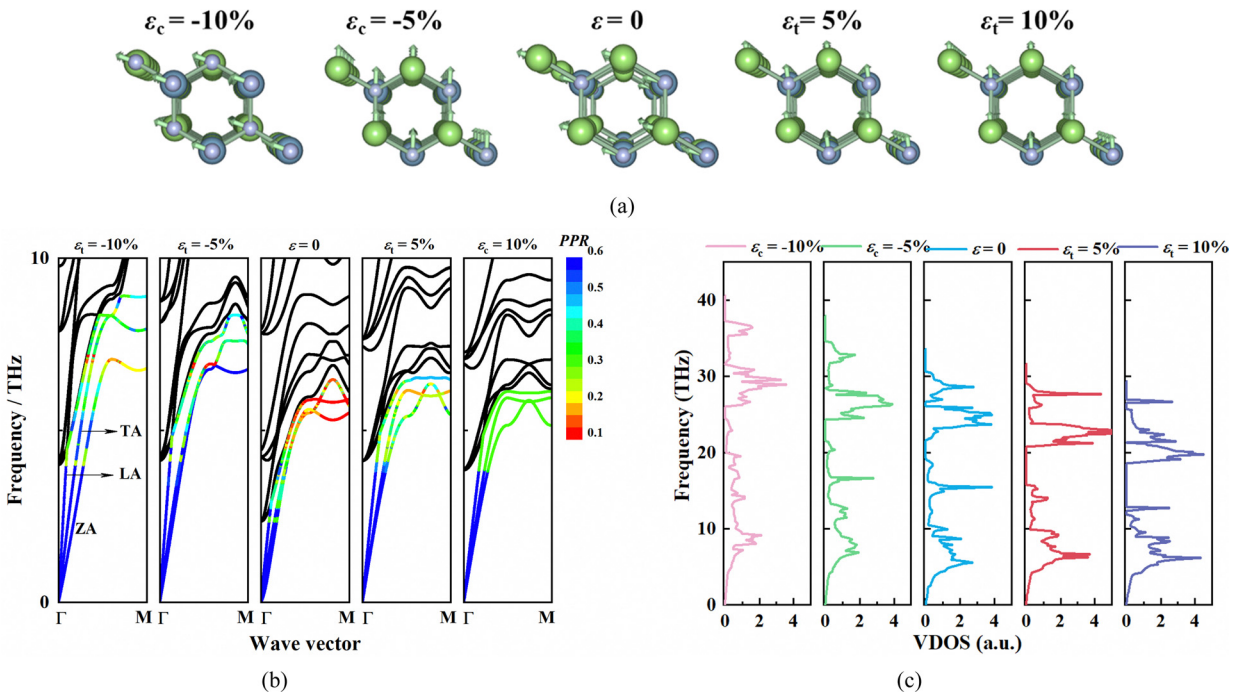

Fig. 5 (a) Visualizing the phonon vibration modes at the 0-point heterojunction, the direction and magnitude of the arrows represent the direction and intensity of lattice vibrations, respectively. (b) Phonon dispersion curves of GaN/AlGaN heterojunctions (with three phonon branches mapping the phonon mode participation rate), (c) dependence of phonon density of states on the in-plane biaxial strain.

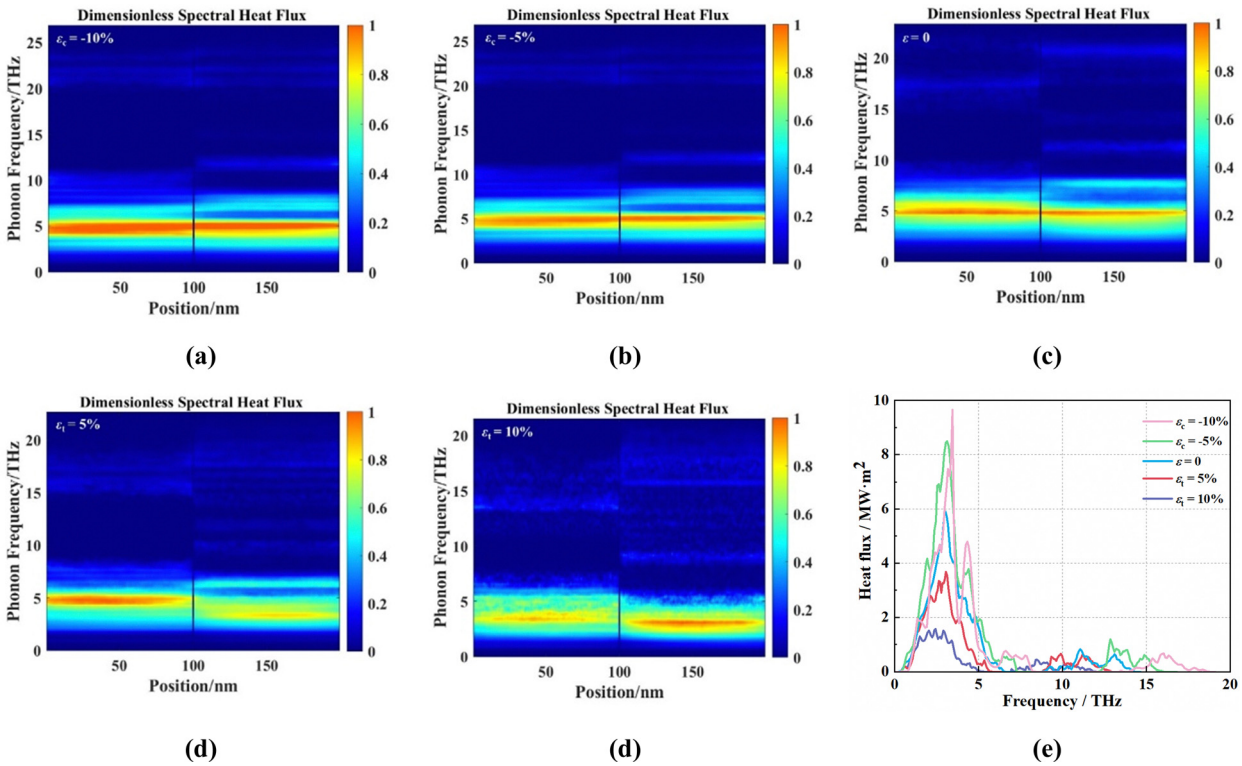

Fig. 6 Strain intensities for (a) ε_c = −10%, (b) ε_c = −5%, (c) ε = 0, (d) ε_t = 5% *vs.* (e) ε_t = 10%, and (e) phonon spectral heat fluxes of GaN/AlGaN at the interface.

component corresponding to the λ order of the positive modes, and N is the total number of atoms. The participation ratio describes the proportion of atoms involved in a specific mode, so it varies between O(1) for delocalized states and O(1/N) for localized states. Observations show that under strain-free conditions, phonons near the M point are significantly localized. Applying compressive or tensile strain can modulate the localized phonons in the heterojunction, making them more easily propagated, and significantly enhance the delocalized phonon modes near the Γ point. Under compressive strain, the phonon cutoff frequency of the heterojunction increases significantly, while the phonon bandgap decreases. When compressive strain is applied, it leads to an increase in bond strength, thereby causing the vibrational frequency of the optical phonon modes to increase, that is, the optical modes shift to higher frequencies. Conversely, under tensile strain, both the phonon cutoff frequency and the phonon bandgap exhibit behavior opposite to that under compressive strain. When tensile strain is applied, the interatomic distances in the heterojunction increase, leading to a decrease in bond strength and a shift of the optical modes to lower frequencies.

In the GaN/AlGaN heterojunction, the impact of strain significantly alters the electron–phonon coupling effect. Observations of changes in the acoustic branches show that, under stress-free conditions, the TA and LA modes exhibit linear dispersion around the highly symmetric Γ point, while the ZA mode displays quadratic dispersion due to rotational symmetry. As the in-plane biaxial compressive strain increases, the parabolic dispersion of the ZA mode transforms into a quasi-linear pattern, and the acoustic phonon branches harden along the Γ–M path. Conversely, under tensile strain, the ZA mode in the Brillouin zone exhibits a softening phenomenon. Further increase of biaxial tensile strain leads to the optical phonons moving towards the low-frequency region of the Brillouin zone, coupling with the acoustic phonon branches. This coupling indicates that phonon propagation in the lattice is disrupted, and phonon–phonon scattering is significantly enhanced. The decrease in frequency and the enhancement of intermodal coupling lead to more frequent phonon–phonon scattering events. This strong scattering effect suppresses the thermal transport capability of phonons, thereby reducing the contribution of electron–phonon coupling to heat conduction. Compressive strain decreases the lattice spacing and enhances the interatomic interaction forces, reducing the chance of phonon scattering, increasing phonon lifetime and group velocity, thus enhancing electron–phonon coupling. Additionally, compressive strain raises the frequency of optical phonons, reducing scattering with low-frequency lattice vibrational modes, and improving the transport efficiency of phonons. The stronger interatomic interaction forces and higher phonon frequencies reduce scattering at the interface, allowing phonons to pass through the interface more effectively. In contrast, tensile strain weakens the interatomic interaction forces and lowers the frequency of optical phonons, thereby hindering interfacial phonon transport.

To delve into the interfacial heat transport mechanisms of the GaN/AlGaN heterostructure under different strain states, we

plotted the phonon spectrum heat flow maps in the frequency domain, as shown in Fig. 6(a)–(d), while Fig. 6(e) illustrates the phonon spectrum heat flow at the interface. These data intuitively reflect the contribution of phonons of different frequencies to interfacial heat transport. The analysis shows that low-frequency phonons dominate the interfacial heat transport process, and within the 2–5 THz frequency range, phonons form a significant interfacial phonon channel. As compressive strain increases, the lattice binding energy is enhanced, enabling more high-frequency phonons to be excited and participate in heat transport, leading to an increase in heat flow density. In contrast, under tensile strain conditions, the lattice binding energy is weakened, and the interaction between phonons and scattering centers increases, limiting the excitation and transport capacity of high-frequency phonons, ultimately resulting in a reduction of heat flow density. These results indicate that changes in the phonon spectrum heat flow significantly affect the regulation of thermal conductivity; the excitation of high-frequency phonons under compressive strain enhances the interfacial thermal conductivity, while tensile strain reduces it. These variations are closely related to the interfacial charge transfer. In the AlGaN/GaN heterojunction, interfacial charge transfer not only affects the transport characteristics of electrons but also alters the electric field distribution at the interface. The presence of strain further affects the intensity and distribution of this charge transfer. Compressive strain reduces electron scattering at the interface by enhancing lattice binding energy, improving thermal conductivity. At the same time, the increased electron density strengthens the coupling between interfacial phonons and

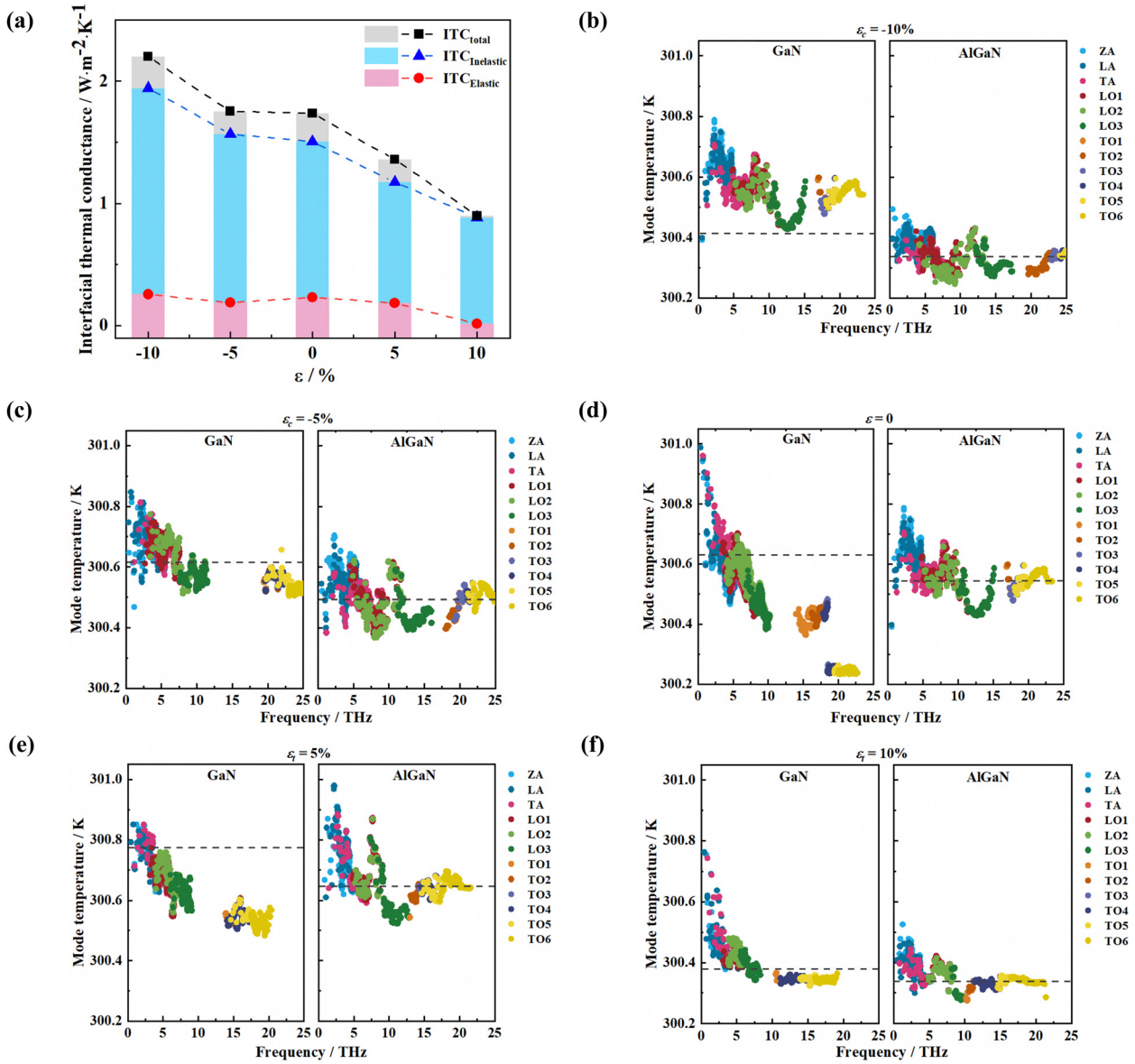

Fig. 7 (a) Strain dependence of ITC. Modal temperatures of GaN and AlGaN on both sides of the interface for stress intensities of (b) $\varepsilon_c = -10\%$, (c) $\varepsilon_c = -5\%$, (d) $\varepsilon = 0$, (e) $\varepsilon_t = 5\%$ and (f) $\varepsilon_t = 10\%$, with the position of dashed line in the figure indicating the equilibrium temperature.

electrons, enhancing heat transport. Furthermore, tensile strain increases the inhomogeneous distribution of interfacial charge, further increasing the complexity and limitations of heat flow.

To investigate the mechanism of in-plane biaxial strain regulating phonon transport at the heterointerface, this section combines the MHHIM model with BTE simulations to study the thermal transport of the GaN/AlGaN interface structure, and provides a detailed description of the strain's regulatory effect on the heterojunction phonons from the perspective of phonons. The thickness (L) from the boundary to the interface is set to 200 nm in the simulation. Fig. 7(a) presents the interfacial thermal conductivity (ITC) obtained from MHHIM simulations, where the black, blue, and pink bars represent the total ITC, and the proportions of elastic and inelastic scattering, respectively. Under stress-free conditions, ITC = 1.74 W m^{-2} K^{-1}. As the in-plane biaxial compressive strain intensity increases, ITC shows a positive correlation trend. When $\varepsilon_c = -10\%$, ITC increases by 26.63%. In contrast, as the in-plane biaxial tensile strain intensity increases, ITC shows a negative correlation trend. When ε_t = 10%, ITC decreases by 48.17%. Furthermore, elastic scattering dominates the transport at the heterojunction interface. Elastic scattering is usually related to the mean free path of phonons, which in turn directly affects the ITC. Under compressive strains, the mean free path of phonons increases due to a decrease in the lattice constant, leading to a decrease in the elastic scattering events and hence an increase in the ITC. Whereas, under tensile strain, the lattice constant increases, the mean free path of phonons decreases and the elastic scattering events increase, leading to a decrease in ITC.

By distinguishing phonon modes, the regulatory process of strain on non-equilibrium phonons at the interface is described in detail. In the BTE solution, the relaxation time approximation is used to solve the equation, ensuring the validity of temperature as an expression of non-equilibrium states. Under steady-state conditions, when heat is transferred from the hot end to the cold end of the structure, phonons of different modes may exhibit different temperature distributions at the same location, known as modal temperature non-equilibrium.[38] To better describe the phonon non-equilibrium phenomenon near the interface, Fig. 7(b)–(f) plot the mode temperature of the phonon branches at the GaN and AlGaN interface as a function of in-plane biaxial strain variation, with the dashed line in the graph representing the equilibrium temperature. For ease of data analysis, 12 different modes of phonons are named ZA, TA, LA, LO1–LO3 (longitudinal optical, longitudinal optical modes), and TO1–TO6 (transverse optical, transverse optical modes) according to the frequency around the Γ point. Observations show that there is a significant temperature difference between phonon modes at the interface, indicating the presence of non-equilibrium phonon transport. Near the interface, compared with the acoustic phonon branches, the temperature of TO and LO phonons drops rapidly. As the compressive strain increases, both the interface temperature and the mode temperature difference decrease. However, when ε_t = 5%, compared with the stress-free state, the interface temperature rises, but the phonon mode temperature difference is greatly increased; when tensile strain continues to increase, the interface temperature is at its lowest. This phenomenon is partly attributed to the weaker degree of phonon non-equilibrium caused by in-plane compressive stress compared to in-plane tensile stress. Due to the lattice structure changes and adjustments in phonon scattering mechanisms caused by strain, the temperature difference between high-temperature acoustic and optical phonons is narrowed. Strain increases the scattering frequency of phonons, and the energy of high-temperature acoustic phonons is more frequently transferred to lower-temperature optical phonons through scattering, thereby reducing the temperature of high-temperature acoustic phonons. At the same time, the temperature of optical phonons rises because they receive more energy. In addition, strain changes the phonon spectrum and heat transfer paths, promoting the redistribution of energy between acoustic and optical phonons, further narrowing their temperature difference. In this way, strain achieves temperature equilibrium between different phonon modes.

As shown in Fig. 8(a), the imbalance in temperature leads to an imbalance in heat flow. The colder phonon branches absorb more energy from the lattice to increase their heat flow, while the hotter phonons lose energy, resulting in a decrease in their heat flow density. As the intensity of in-plane biaxial tensile strain increases, the heat flow of the acoustic branches on the AlGaN side is enhanced, while the heat flow of the optical branches is significantly weakened. This imbalance in heat flow is caused by energy transfer between phonons and the non-equilibrium state. As the intensity of in-plane biaxial tensile strain increases, the heat flow of AlGaN side acoustic phonons is enhanced, while the heat flow of optical phonons is significantly weakened. This is because tensile strain changes the lattice structure and phonon scattering mechanisms, leading to reduced scattering of acoustic phonons, increased lifetime, higher thermal conductivity, and thus enhanced heat flow. Optical phonons, due to frequent inelastic scattering, have a reduced lifetime and lower heat flow density. In addition, tensile strain causes changes in the phonon spectrum and adjustments in energy distribution, increasing the kinetic energy of acoustic phonons and their heat-carrying capacity, while the energy of optical phonons is lost to other phonon modes, reducing the heat flow. Ultimately, the impact of tensile strain on lattice dynamics makes acoustic phonons more adaptable to the new lattice structure, while the conduction path of optical phonons is obstructed, leading to a reduction in their heat flow.

Furthermore, the BTE was used to solve the impact of strain on the quasi-steady-state transport properties of phonons, and the ballistic part in the heat transport process was calculated. The calculated ballistic phonon energy density of GaN/AlGaN modes as a function of in-plane biaxial strain is shown in Fig. 8(b). Observations show that there are fewer ballistic phonons inside the material, and more near the boundaries and interfaces. The ballistic phonons decrease sharply from the boundaries or interfaces to the interior, where phonons undergo scattering and lose their ballistic characteristics. Phonons have a higher group velocity and longer relaxation time, meaning they are not as prone to scattering in the material as optical phonons. This indicates that when phonons have more

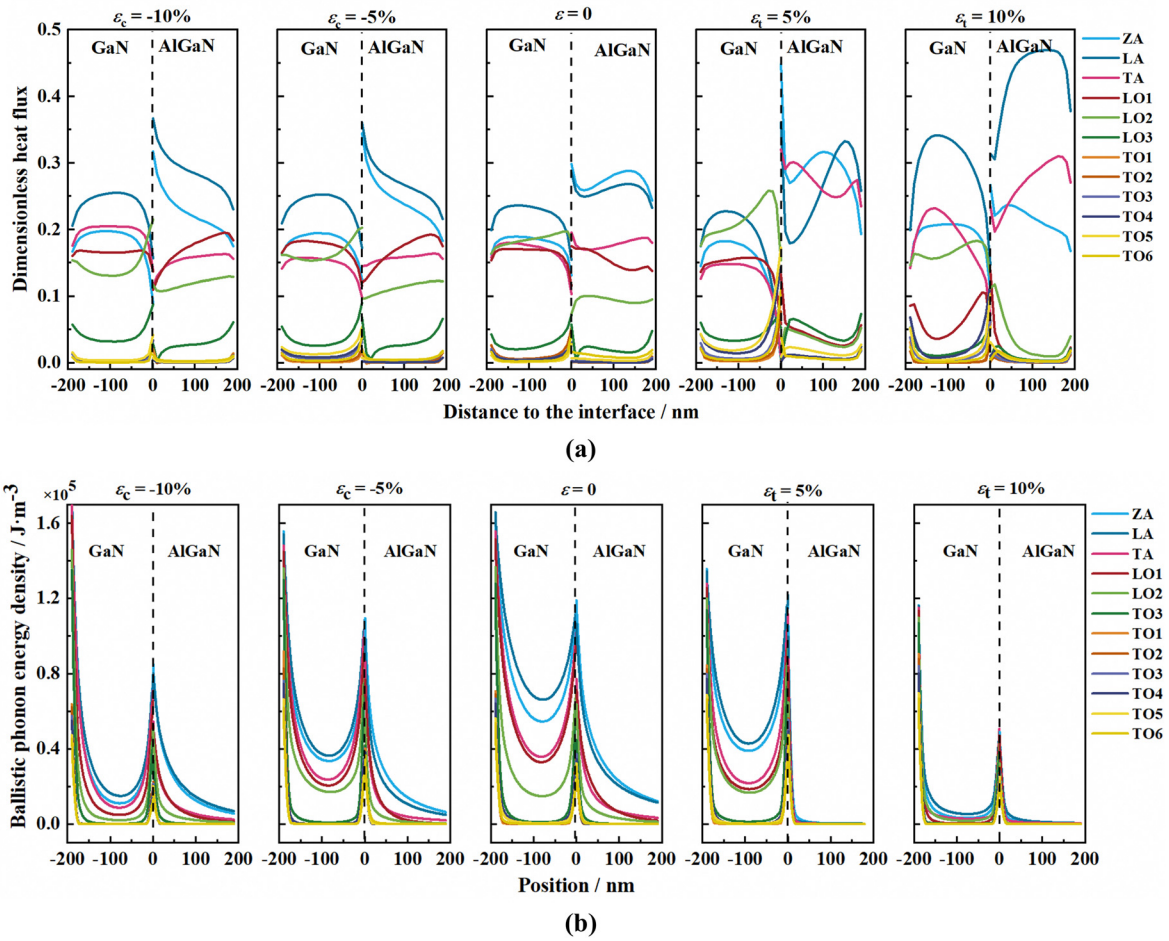

Fig. 8 Variation with in-plane biaxial strain of (a) phonon branch contribution to heat flow, (b) GaN/AlGaN modal ballistic phonon energy density.

energy, ballistic transport is stronger. Additionally, the energy density of ballistic phonons in the acoustic branches is higher than in the optical branches, with low-frequency phonons dominating the interfacial phonon transport. Under the action of in-plane biaxial stress, the ballistic phonon transport at the interface is severely suppressed. This is because low-frequency phonons have longer wavelengths and lower energy, and under stress-free conditions, they can pass through the interface more freely. However, when in-plane biaxial stress is applied, the lattice structure changes, leading to an increase in phonon scattering rates. The lattice distortion and irregularity caused by stress disrupt the paths of phonons, reducing the possibility of ballistic transport. Ultimately, this leads to the suppression of ballistic transport of low-frequency phonons, and the overall heat flow of phonons is significantly affected.

4. Conclusions

This study, through the integrated application of first-principles calculations and simulations based on the Boltzmann transport equation (BTE), deeply investigated the heat transport mechanisms of GaN/AlGaN heterojunctions under in-plane stress, revealing the complexity of electron–electron scattering, phonon ballistics, non-equilibrium processes, and electron–phonon coupling transport. The research results indicate that strain is an effective means of regulating the thermoelectric properties of semiconductor materials.

Firstly, this study utilized EPW software and DFT calculations to analyze the impact of strain on the electron–phonon coupling constant and scattering rate. The results show that strain significantly modulates the degree of e–ph coupling, with compressive strain enhancing the coupling and tensile strain weakening the interaction.

Secondly, we delved into the influence of in-plane stress on the electron transport behavior of the GaN/AlGaN heterojunction. By calculating the ELF, we observed that strain significantly altered the spatial distribution of electrons, with electrons being highly delocalized near Ga and Al atoms and mainly localized near N atoms. In-plane biaxial strain led to a decrease in ELF values, indicating that strain reduced the degree of electron localization around Ga atoms, and both compressive and tensile strains decreased the degree of electron localization. Furthermore, the higher work function of AlGaN compared to GaN causes electrons to migrate from AlGaN to GaN, forming a two-dimensional electron gas. Compressive strain increased the difficulty for

electrons to escape, raising the work function, while tensile strain reduced it. Through the analysis of three-dimensional charge difference density, we found that under strain conditions, there was a reallocation of charge at the interface, with a large number of electrons transferring from AlGaN to GaN, forming a two-dimensional electron gas, and the phenomenon of charge depletion decreased with increasing strain.

Lastly, through the MHHIM model and BTE simulations, we detailed the response of interfacial phonon non-equilibrium and quasi-ballistic transport to strain. The phonon density of states and dispersion curves indicate that strain significantly altered the lattice vibrational modes, with compressive strain increasing the phonon cutoff frequency and narrowing the phonon bandgap, while tensile strain had the opposite effect. Moreover, strain enhanced the delocalized phonon modes near the Γ point. Under compressive strain, the increase in bond strength led to an increase in optical phonon frequencies, while under tensile strain, the increase in atomic spacing weakened the bond strength, reducing the optical phonon frequencies. Analysis through the phonon spectrum heat flow map in the frequency domain revealed that low-frequency phonons dominate interfacial heat transport, with compressive strain enhancing the interfacial thermal conductivity and tensile strain reducing it. The degree of phonon non-equilibrium caused by in-plane compressive stress is weaker than that caused by in-plane tensile stress. Additionally, under the action of in-plane biaxial stress, the ballistic phonon transport at the interface is severely suppressed. In summary, this study not only enriched the understanding of electron–phonon coupling phenomena in GaN/AlGaN heterojunctions but also provided a theoretical basis and guidance for the strain design and device application of semiconductor materials.

Data availability

The data that support the findings of this study are available from the corresponding author, upon reasonable request.

Conflicts of interest

There are no conflicts to declare.

Acknowledgements

We acknowledge funding supports from the National Natural Science Foundation of China (52276089 and U22A20210) and Natural Science Foundation of Shandong Province (grant no. ZR2023ZD18).

References

1 A. J. Schmidt, X. Chen and G. Chen, Pulse accumulation, radial heat conduction, and anisotropic thermal conductivity in pump–probe transient thermoreflectance, *Rev. Sci. Instrum.*, 2008, **79**(11), 114902.
2 J. A. Rowlette and K. E. Goodson, Fully Coupled Nonequilibrium Electron–Phonon Transport in Nanometer-Scale Silicon FETs, *IEEE Trans. Electron Devices*, 2008, **55**(1), 220–232.
3 J. Osvald, Polarization effects and energy band diagram in AlGaN/GaN heterostructure, *Appl. Phys. A: Mater. Sci. Process.*, 2007, **87**(4), 679–682.
4 O. Ambacher, B. Foutz, J. Smart, J. R. Shealy, N. G. Weimann, K. Chu, M. Murphy, A. J. Sierakowski, W. J. Schaff, L. F. Eastman, R. Dimitrov, A. Mitchell and M. Stutzmann, Two dimensional electron gases induced by spontaneous and piezoelectric polarization in undoped and doped AlGaN/GaN heterostructures, *J. Appl. Phys.*, 2000, **87**(1), 334–344.
5 S. V. Novikov, C. R. Staddon, R. W. Martin, A. J. Kent and C. T. Foxon, Molecular beam epitaxy of free-standing wurtzite Al Ga1–N layers, *J. Cryst. Growth*, 2015, **425**, 125–128.
6 H. P. Lee, J. Perozek, L. D. Rosario and C. Bayram, Investigation of AlGaN/GaN high electron mobility transistor structures on 200-mm silicon (111) substrates employing different buffer layer configurations, *Sci. Rep.*, 2016, **6**, 37588.
7 S. Sun, X. Xie, P. Zhang, Z. Zhao, J. Wei and X. Luo, Improvement of single event transients effect for a novel AlGaN/GaN HEMT with enhanced breakdown voltage, *J. Sci.: Adv. Mater. Devices*, 2024, **9**(2), DOI: **10.1016/j.jsamd.2024.100692**.
8 B. Mounika, J. Ajayan, S. Bhattacharya and D. Nirmal, Recent developments in materials, architectures and processing of AlGaN/GaN HEMTs for future RF and power electronic applications: A critical review, *Micro Nanostruct.*, 2022, **168**, 207317.
9 L. Li, A. Fukui and A. Wakejima, Bonding GaN on high thermal conductivity graphite composite with adequate interfacial thermal conductance for high power electronics applications, *Appl. Phys. Lett.*, 2020, **116**, 142105.
10 V. Thirunavukkarasu, Y.-R. Jhan, Y.-B. Liu and Y.-C. Wu, Performance of Inversion, Accumulation, and Junctionless Mode n-Type and p-Type Bulk Silicon FinFETs With 3-nm Gate Length, *IEEE Electron Device Lett.*, 2015, **36**(7), 645–647.
11 B. Liao, B. Qiu, J. Zhou, S. Huberman, K. Esfarjani and G. Chen, Significant reduction of lattice thermal conductivity by the electron–phonon interaction in silicon with high carrier concentrations: a first-principles study, *Phys. Rev. Lett.*, 2015, **114**(11), 115901.
12 J. Xu, Y. Hu and H. Bao, Quantitative Analysis of Nonequilibrium Phonon Transport Near a Nanoscale Hotspot, *Phys. Rev. Appl.*, 2023, **19**, 014007.
13 T. Feng, Y. Zhong, J. Shi and X. Ruan, Unexpected high inelastic phonon transport across solid–solid interface: Modal nonequilibrium molecular dynamics simulations and Landauer analysis, *Phys. Rev. B*, 2019, **99**, 045301.
14 B. Hu, W. Bao, G. Chen, Z. Wang and D. Tang, Boltzmann transport equation simulation of phonon transport across GaN/AlN interface, *Comput. Mater. Sci.*, 2023, **230**, 112485.
15 H. A. Yang and B. Y. Cao, Mode-resolved phonon transmittance using lattice dynamics: Robust algorithm and statistical characteristics, *J. Appl. Phys.*, 2023, **134**, 155302.

16 D. S. Tang, G. Z. Qin and M. Hu, *et al.*, Thermal transport properties of GaN with biaxial strain and electron–phonon coupling, *J. Appl. Phys.*, 2020, **127**(3), 035102.
17 X. Yang, A. Jena, F. Meng, S. Wen, J. Ma, X. Li and W. Li, Indirect electron–phonon interaction leading to significant reduction of thermal conductivity in graphene, *Mater. Today Phys.*, 2021, **18**, 100315.
18 Y. Chen, J. Ma and W. Li, Understanding the thermal conductivity and Lorenz number in tungsten from first principles, *Phys. Rev. B*, 2019, **99**, 020305.
19 H. Liu, C. Yang, B. Wei, L. Jin, A. Alatas, A. Said, S. Tongay, F. Yang, A. Javey, J. Hong and J. Wu, Anomalously Suppressed Thermal Conduction by Electron–Phonon Coupling in Charge-Density-Wave Tantalum Disulfide, *Adv. Sci.*, 2020, **7**(11), 1902071.
20 S. Rasheed, S. Ahmad, B. Amin, F. Khan, T. Nasir, M. Ilyas and I. Ahmad, Strain effect on the electronic and photocatalytic properties of GaN-MSSe (M = Mo, W), *J. Solid State Chem.*, 2022, **306**, 122798.
21 Y. Cao, Q. Guan, W. Jia, X. Wang, L. Zhang, Y. He and E. Li, Effect of strain on the effective mass of GaN and the mobility of AlGaN/GaN two-dimensional electron gas, *Mater. Today Commun.*, 2023, **35**, 105788.
22 S. Kong, H. Lim, A. Hoessinger and E. Guichard, P-131: TCAD Modeling of Mechanical Stress for Simulation of Thin Film Transistor on Flexible Substrate, SID Symposium Digest of Technical Papers, 50(1) (2019) 1606–1609.
23 B. K. Labani and W. A. Diery, First-principles study on electronic structure and optical properties of monolayer Janus PtSTe under external electric field and strain, *Eur. Phys. J. Plus*, 2021, **136**, 1197.
24 R. Kaur and N. R. Mohapatra, Process-induced uniaxial strain in Nanosheet-FET based CMOS technology – Is it still beneficial? in: 2023 7th IEEE Electron Devices Technology & Manufacturing Conference (EDTM), 2023, pp. 1–3.
25 L. Zhu and H. Luo, Phonon properties and thermal conductivity of GaN nanofilm under prestress and surface/interface stress, *J. Alloys Compd.*, 2016, **685**, 619–625.
26 S. Nag, R. Singh and R. Kumar, Strain-induced enhancement in the electronic and thermal transport properties of the tin sulphide bilayer, *Phys. Chem. Chem. Phys.*, 2021, **24**(1), 211–221.
27 T. Zhou, G. Qian, S. Huang, Q. Liang, X. Luo and Q. Xie, The effect of biaxial strain on the electronic structures and optical properties of GaS/SSnSe heterojunction: A first-principles calculations, *Phys. Lett. A*, 2023, **480**, 128956.
28 J. Song, Z. Ding, X.-F. Liu, Z.-C. Huang, J.-W. Li, J.-M. Wei, Z.-J. Luo, J.-H. Wang and X. Guo, The effect of biaxial tensile strain on structure and photoelectric properties of Fe-doped GaN monolayer, *Comput. Mater. Sci.*, 2021, **197**, 110644.
29 S. Poncé, E. R. Margine, C. Verdi and F. Giustino, EPW: Electron–phonon coupling, transport and superconducting properties using maximally localized Wannier functions, *Comput. Phys. Commun.*, 2016, **209**, 116–133.
30 S. Ponce, E. R. Margine, C. Verdi and F. Giustino, EPW: Electron–phonon coupling, transport and superconducting properties using maximally localized Wannier functions, *Comput. Phys. Commun.*, 2016, **209**, 116–133.
31 G. Kresse and J. Furthmüller, Efficient iterative schemes for *ab initio* total-energy calculations using a plane-wave basis set, *Phys. Rev. B: Condens. Matter Mater. Phys.*, 1996, **54**(16), 11169.
32 P. E. Blochl, Projector augmented-wave method, *Phys. Rev. B: Condens. Matter Mater. Phys.*, 1994, **50**(24), 17953–17979.
33 A. J. H. McGaughey, A. Jain, H.-Y. Kim and B. Fu, Phonon properties and thermal conductivity from first principles, lattice dynamics, and the Boltzmann transport equation, *J. Appl. Phys.*, 2019, **125**, 011101.
34 A. Togo and I. Tanaka, First principles phonon calculations in materials science, *Scr. Mater.*, 2015, **108**, 1–5.
35 W. Li, J. Carrete, N. A. Katcho and N. Mingo, ShengBTE: A solver of the Boltzmann transport equation for phonons, *Comput. Phys. Commun.*, 2014, **185**(6), 1747–1758.
36 P. E. Hopkins, Multiple phonon processes contributing to inelastic scattering during thermal boundary conductance at solid interfaces, *J. Appl. Phys.*, 2009, **106**, 013528.
37 M. Mohamadi, M. A. Mehrabian and A. Raisi, Heat transfer modelling in the Si–Ge nanoparticle composites by numerical solution of the equation of phonon radiative transfer, *Micro Nano Lett.*, 2018, **13**(6), 788–793.
38 A. Marini, S. Poncé and X. Gonze, Many-body perturbation theory approach to the electron–phonon interaction with density-functional theory as a starting point, *Phys. Rev. B: Condens. Matter Mater. Phys.*, 2015, **91**, 224310.
39 M. Calandra, G. Profeta and F. Mauri, Adiabatic and non-adiabatic phonon dispersion in a Wannier function approach, *Phys. Rev. B: Condens. Matter Mater. Phys.*, 2010, **82**, 165111.
40 J. Quereda, P. San-Jose, V. Parente, L. Vaquero-Garzon, A. J. Molina-Mendoza, N. Agraït, G. Rubio-Bollinger, F. Guinea, R. Roldán and A. Castellanos-Gomez, Strong Modulation of Optical Properties in Black Phosphorus through Strain-Engineered Rippling, *Nano Lett.*, 2016, **16**(5), 2931–2937.
41 J. H. Lee, M. H. Kang, S. C. Yi, J. H. Park and N. Oh, Counterbalancing effects of bowing in gallium nitride templates by epitaxial growth on pre-strained sapphire substrates, *Ceram. Int.*, 2024, **50**(22), 47666–47676.
42 Y. Ni, L. Li, L. He, T. Que, Z. Liu, L. He, Z. Wu and Y. Liu, Dependence of carbon doping concentration on the strain-state and properties of GaN grown on Si substrate, *Superlattices Microstruct.*, 2018, **120**, 720–726.
43 F. J. Himpsel, G. Hollinger and R. A. Pollak, Determination of the Fermi-level pinning position at Si(111) surfaces, *Phys. Rev. B: Condens. Matter Mater. Phys.*, 1983, **28**(12), 7014–7018.
44 S. Hu, Z. Zhang, P. Jiang, W. Ren, C. Yu, J. Shiomi and J. Chen, Disorder limits the coherent phonon transport in two-dimensional phononic crystal structures, *Nanoscale*, 2019, **11**(24), 11839–11846.